Materials Today Bio 23 (2023) 100887

Contents lists available at ScienceDirect

Materials Today Bio

journal homepage: www.journals.elsevier.com/materials-today-bio

IOX1 epigenetically enhanced photothermal therapy of 3D-printing silicene scaffolds against osteosarcoma with favorable bone regeneration

Yimin Liang [a,1], Chunmeng Wang [b,1], Shiyang Yu [c,1], Yujia Fan [d], Yuhang Jiang [c], Renpeng Zhou [a,**], Wangjun Yan [b,***], Yangbai Sun [b,*]

[a] Department of Plastic and Reconstructive Surgery, Shanghai Ninth People's Hospital, School of Medicine, Shanghai Jiao Tong University, Shanghai, 200011, China
[b] Department of Musculoskeletal Oncology, Fudan University Shanghai Cancer Center, Shanghai, 200032, China
[c] Department of Orthopedics, Shanghai Sixth People's Hospital, School of Medicine, Shanghai Jiao Tong University, Shanghai, 200233, China
[d] Department of Stomatology, Shanghai Xuhui District Dental Center, Shanghai, 200032, China

ARTICLE INFO

Keywords:
Silicene
Osteosarcoma
3D-printing
Photothermal therapy
Bone regeneration
IOX1

ABSTRACT

Osteosarcoma (OS) is the third most common malignancy in adolescence. Currently, the treatments of OS confront great obstacles of tumor recurrence and critical bone defects after surgery, severely affecting the survival rates and living qualities of patients. Hence, it is urged to develop distinct biomaterials with both efficient tumor therapeutic and osteogenic functions. Although photothermal therapy (PTT) has aroused expanding interest, characterizing negligible invasiveness and high spatiotemporal adjustment, few studies discussed its drawbacks, such as thermal injury to adjacent normal tissue and exceeded laser power density, implying that focusing on sensitizing OS to PTT instead of simply elevating the laser power density may be a fresh way to enhance the PTT efficacy and attenuate the side/adverse effects. Herein, we successfully constructed 3D-printing silicene bioactive glass scaffolds with preferable PTT efficacy at the second near-infrared (NIR-II) biowindow and outstanding osteogenic biofunctions owing to the release of bioactive elements during degradation. Impressively, a histone demethylase inhibitor, IOX1, was introduced before PTT to sensitize OS to thermal therapy and minimize the side/adverse effects. This work offered a distinctive paradigm for optimizing the PTT efficacy of osteogenic scaffolds against OS with epigenetic modulation agents.

1. Introduction

Osteosarcoma (OS) is one of the most frequent primary bone tumors in children and adolescents, with an incidence of 8–11 per million yearly at 15–19 years old [1]. Meanwhile, it is also the third most common malignancy in adolescence, behind lymphomas and brain cancers [2,3]. Currently, the effective therapeutic modalities for bone tumors include surgical resection, chemotherapy, and radiotherapy [4]. The surgery is often limited to obliterating the tumor entirely owing to the invasive nature of bone malignancies. Meanwhile, the critical bone defect after surgery is beyond the self-healing ability, which needs the help of osteogenic biomaterials [5]. Speaking of the chemotherapy of OS, it still relies on the same drugs as in the early 1980s, and the survival rates have plateaued since the 1990s [3,6]. In addition, chemotherapy is often accompanied by severe adverse/side effects and leads to drug resistance [7]. Hence, it is highly urgent to explore distinct multifunctional prostheses which can efficiently realize the elimination of the residual tumor cells to suppress tumor recurrence and possess remarkable bone reconstruction capacity [8,9].

In recent studies, photothermal therapy (PTT) has garnered more and more attention for tumor therapy because of its spatiotemporal adjustable feature with high efficiency and minimal side effects [10–12]. Up to now, many photothermal agents have been reported, including carbon-based materials, metal disulfides, organic nanostructures, and gold nanoparticles [13,14]. However, carbon-based materials possessed unsatisfactory biocompatibility [15]. Metal disulfides and gold nanoparticles are difficult to biodegrade [16]. These drawbacks limit their biomedical applications. By contrast, two-dimensional (2D) silicene

* Corresponding author.
** Corresponding author.
*** Corresponding author.
E-mail addresses: renpengzhou@126.com (R. Zhou), yanwj@fudan.edu.cn (W. Yan), drsunyb@fudan.edu.cn (Y. Sun).
[1] These authors contributed equally to this work.

https://doi.org/10.1016/j.mtbio.2023.100887
Received 4 October 2023; Received in revised form 19 November 2023; Accepted 27 November 2023
Available online 30 November 2023

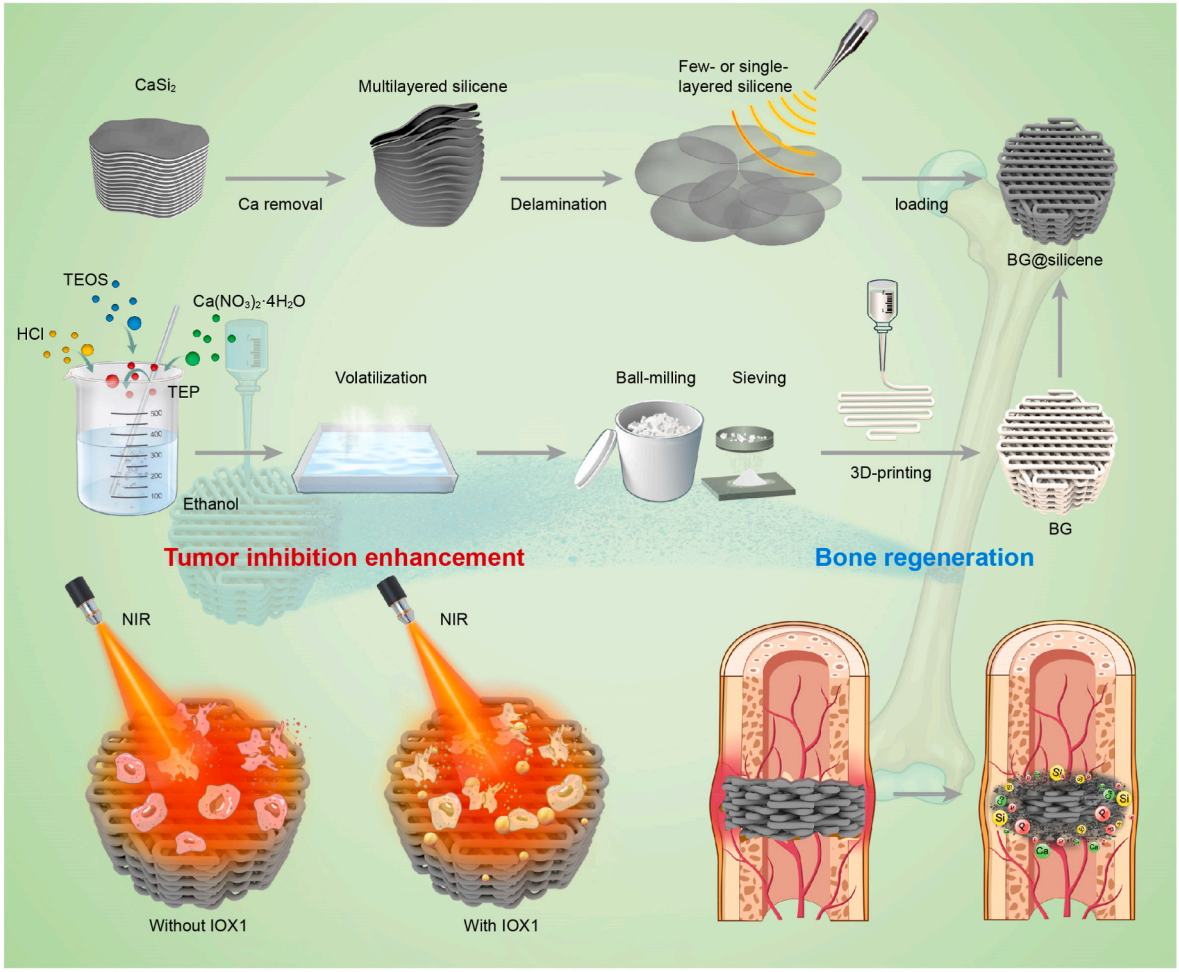

Fig. 1. Scheme describing the construct of 3D-printing silicene scaffolds (BG@silicene) to realize both enhanced residual OS ablation in NIR-II biowindow facilitated by IOX1 and promoted bone regeneration. Notably, an inhibitor of histone demethylase, IOX1, was administrated before PTT to strengthen the therapeutic efficacy and minimize the adverse/side effects.

nanosheets (NSs) featured satisfactory biosafety and biodegradability and had profound photonic hypothermia against breast cancer in the first near-infrared (NIR-I) biowindow [17]. However, their therapeutic capabilities to ablate OS in the second near-infrared (NIR-II) biowindow and promote osteogenesis have not been explored, which deserves further evaluation. Besides, compared to NIR-I biowindow (650–1000 nm), NIR-II biowindow (1000–1350 nm) penetrated deeper into the tissue and could be tolerated more by the skin [18,19]. Thus, it is more attractive to exploit NIR-II photothermal agents integrated multifunctional scaffolds to cure OS-caused bone defects.

Three-dimensional (3D)-printing bioactive glass (BG) scaffolds are characterized by precisely controlled internal structure, connected macropores, favorable degradation rate, satisfactory biosafety, and pleasing osteoconductivity/osteoinductivity [20–22]. Therefore, the modification of 3D porous BG scaffolds with 2D silicene NSs is anticipated to form a multifunctional platform with photonic hyperthermia and improved osteogenic functionalities.

Despite tremendous efforts that have been made in PTT, there are still some aspects that need to be optimized. For example, the high temperature induced by photonic hyperthermia would inevitably cause damage to the surrounding normal tissue. Hence, upregulating the sensitivity of tumors to the PTT would be a feasible solution to enhance the therapeutic efficacy and weaken the side effects simultaneously. Unfortunately, few studies focused on promoting PTT's therapeutic sensitivity. It has been reported that the downregulation of lysine demethylase KDM3A would sensitize breast cancer to photothermia epigenetically [17]. Thus, it can be inferred that KDM3A may also potentially mediate the sensitivity of PTT to OS, and inhibition of the enzyme activity of KDM3A might benefit PTT.

Herein, a simple and efficient platform was constructed by modifying the ultrathin silicene NSs onto the 3D-printing BG scaffolds (BG@silicene) to realize both enhanced residual OS ablation in NIR-II biowindow facilitated by IOX1 and promoted bone regeneration whereafter (Fig. 1). Noteworthy, 5-carboxy-8-hydroxyquinoline (IOX1), an inhibitor of histone demethylase KDM3A [23], was administrated before PTT, which attempted to strengthen the therapeutic efficacy. In addition, the released bioactive components (*e.g.*, calcium, silicon, phosphate, *etc.*) from the gradual degradation of BG@silicene scaffolds prompted osteogenesis by stimulating the proliferation, differentiation, and mineralization of bone mesenchymal stem cells [24]. Taken together, the reported BG@silicene scaffold offered a distinctive paradigm for optimizing the PTT efficacy of osteogenic scaffolds against OS with epigenetic modulation agents.

2. Experimental section

2.1. Synthesis of 3D-printing BG@silicene scaffolds and their characterization

The 3D-printing BG scaffolds and silicene NSs were constructed as reported [17,20]. For obtaining BG@silicene scaffolds, the BG scaffolds were soaked in the indicated concentration of silicene NSs aqueous

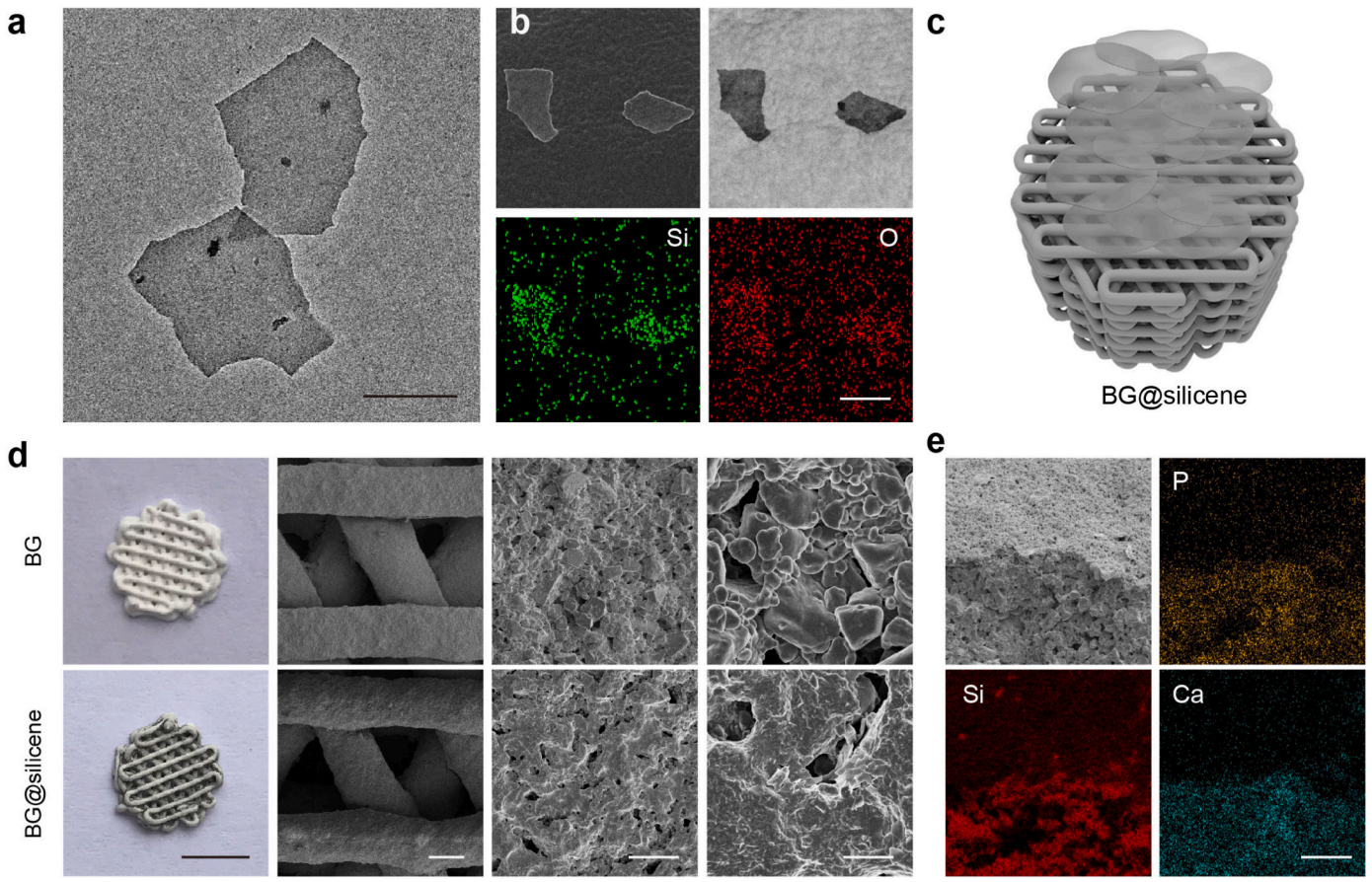

Fig. 2. Construction and constitution features of BG@silicene scaffolds. (a) The TEM image of ultrathin silicene NSs. Scale bar, 200 nm. (b) SEM pictures and related elements distributions of silicene NSs. Scale bar, 200 nm. (c) Scheme to illustrate the preparation of BG@silicene scaffolds. (d) Digital and SEM photos of BG scaffold (upper row) and BG@silicene scaffold (lower row). Scale bar from left to right, 4 mm, 200 μm, 10 μm, and 1 μm). (e) Surface morphology and elements distributions of a fractured BG@silicene scaffold. Scale bar, 10 μm.

solution (400 ppm without additional notes) for 10 min and then put in the drier (37 °C) for 5 h. The above steps were repeated three times. The scaffolds were sterilized with ethylene oxide before being applied *in vitro* and *in vivo*.

Transmission electron microscopy (TEM) and thermal images were recorded by JEM-2100F and FOTRIC 228S, respectively. The morphological images and elemental mapping were obtained from a scanning electron microscope (Magellan 400). Atomic force microscope (AFM) analysis was measured by NTEGRA Spectra II system.

2.2. In vitro cytocompatibility and OS suppression assays

The human OS cells, 143B and HOS, were purchased from American Type Culture Collection. The cells were cultured in Dulbecco's modified Eagle medium (DMEM) with antibiotics (100 U·mL^{-1} penicillin and 100 μg·mL^{-1} streptomycin) and 10% fetal bovine serum (Gibco, USA) in a humidified atmosphere with 5% CO_2 at 37 °C. For the *in vitro* cytocompatibility assay, OS cells and mouse bone mesenchymal stem cells (mBMSCs) were seeded on the indicated scaffolds for 24 or 48 h, and the cell counting kit-8 (CCK8) assay was executed following the instructions [25]. For OS suppression assay in NIR-II biowindow, OS cells were seeded on the indicated scaffolds for 6 h to ensure cellular attachment. Then, IOX1 was given to the related group for 24 h. Afterward, laser irradiation (1064 nm, 0.8 W·cm^{-2}, 5 min) was executed in the corresponding group. The CCK8 assay or the flow cytometry was conducted 24 h later [26,27].

2.3. Osteogenic differentiation in vitro

mBMSCs seeded on the indicated scaffolds were cultured in the standard or osteoinductive medium (OIM) for 7 days. Afterward, the ALP activity assay and RT-qPCR were performed following the instructions reported before [12,28–30]. The information on the primers is provided in Supplementary Table S1.

2.4. Animals

All animal procedures were approved by the Ethics Committee of Shanghai Medical College Fudan University.

For *in vivo* biosafety analysis, fifteen ICR mice (6–8 weeks) were purchased from Jiesijie Laboratory Animal Center (Shanghai, China). The mice were randomly divided into three groups. Besides the untreated group, the other two groups were subcutaneously implanted with the BG and BG@silicene scaffolds, respectively. Then, the mice were raised under specific pathogen-free (SPF) conditions for 30 days. After that, their blood and major organs were collected for biosafety evaluations.

For the *in vivo* PTT efficacy evaluation, twenty nude male BALB/c mice (6–8 weeks) were purchased from Silaike (Shanghai, China). First, 1×10^6 143B cells were injected subcutaneously into mice to establish an ectopic OS model. When the tumor volume reached 100 cm^3, the mice were randomly divided into four groups: BG + NIR, IOX1 + BG, PTT, and IOX1 + PTT. IOX1 (5 mg·kg^{-1}) was administrated intraperitoneally 20 h before the scaffold implantation surgeries. The scaffolds were implanted into the center of the tumor, and the laser irradiation

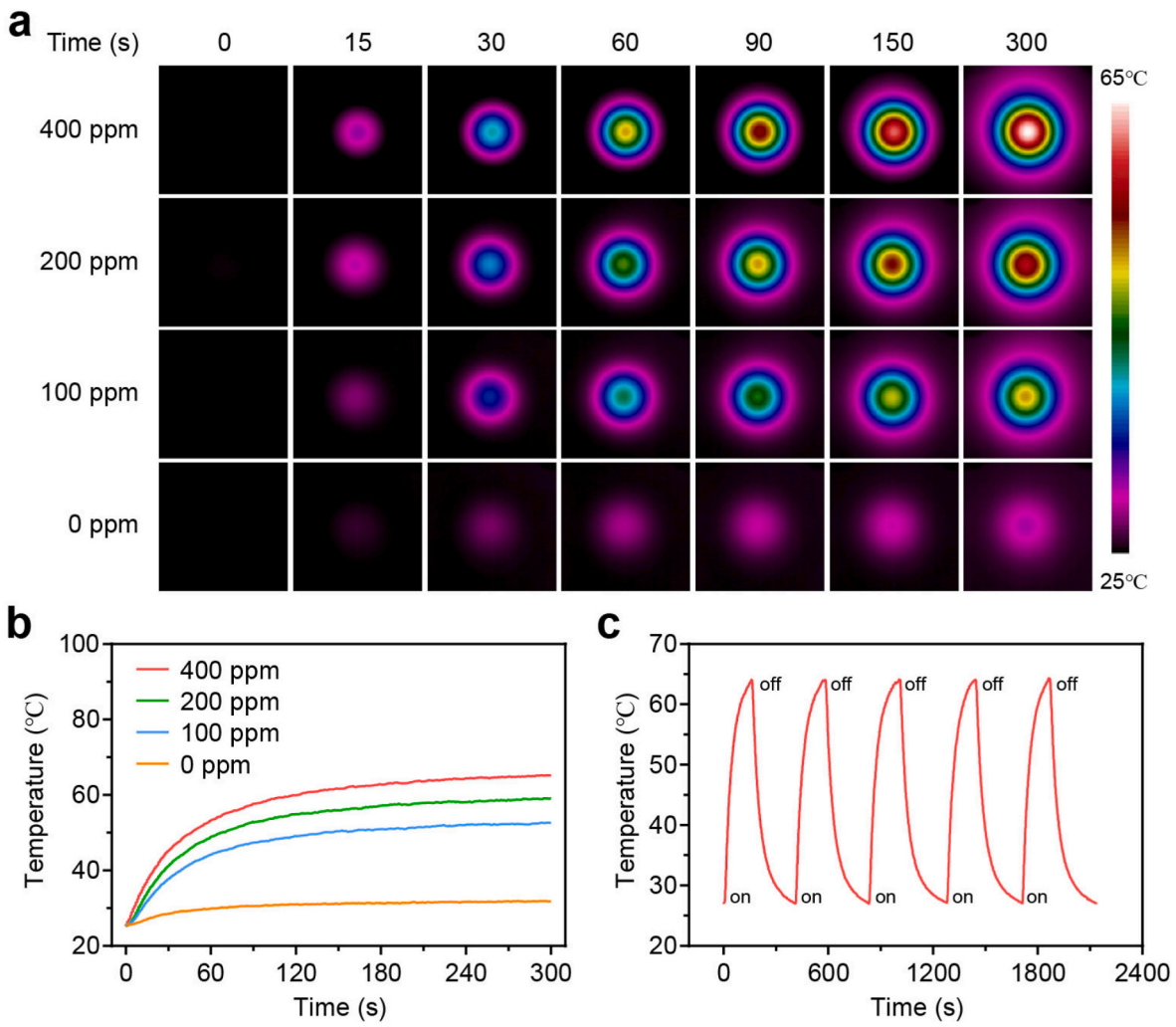

Fig. 3. Photothermal characteristics of BG@silicene scaffolds. The photothermal (a) images and (b) curves of BG@silicene scaffolds loading different amounts of silicene NSs when exposed to 1064 nm laser irradiation (1.0 W·cm^{-2}). (c) Photothermal curves of the BG@silicene (400 ppm) scaffold exposed to 1064 nm laser irradiation (1.0 W·cm^{-2}) for five irradiation-on/off cycles.

(1064 nm, 0.8 W·cm^{-2}, 10 min) was executed in BG + NIR, PTT, and IOX1 + PTT groups 4 h after the implantation surgeries. Later, the tumor volume was measured every 4 days for 12 days. After the mice were sacrificed, the tumors were resected, photographed, weighed, and subjected to further histochemistry analyses.

2.5. In vivo osteogenic analysis of BG@silicene scaffolds

Ten male Sprague-Dawley (SD) rats (8 weeks) were purchased from Silaike (Shanghai, China). The calvarial defect model was utilized to elevate the osteogenic property of scaffolds. First, the rats were anesthetized, and the skin of the skull was sterilized. Second, an incision was made on the calvarial sagittal suture. Third, 10-mm-diameter defects were drilled on the frontoparietal bone by an electric trephine. Fourth, the BG or BG@silicene scaffolds were implanted in the defects. Last, the periosteum and skin were sutured sequentially. The alizarin red and calcein were injected subcutaneously at weeks 6 and 7, respectively. The rats were euthanized at week 8, and their calvaries were resected for further histochemistry analyses.

2.6. Data

The mean, standard deviation (SD), and p values based on two-tailed t-tests were calculated with Excel (Microsoft). Differences were regarded as significant at $p < 0.05$ (*$p < 0.05$, **$p < 0.01$).

3. Results and discussion

3.1. Construction and constitution features of BG@silicene scaffolds

Firstly, 2D silicene NSs were obtained through a mild oxidation process followed by ultrasonic exfoliation [17]. The constructed silicene NSs exhibited ultrathin microstructures and were about 200 nm in plan view scale, as shown in TEM images (Fig. 2a). The thickness of silicene NSs was about 7–12 nm tested by the AFM, reiterating their ultrathin structure (Supplementary Fig. S1). Moreover, the elements mapping results implied the uniformly distributed silicon and oxygen elements in/on the silicene NSs (Fig. 2b). By the way, the presence of oxygen elements is attributed to the mild oxidation process during the construction of silicene NSs.

In general, interconnected pores for cell ingrowth and nutrition transportation are pivotal for preparing bone scaffolds [31]. However, the reported techniques, such as gas foaming and polyurethane foam templating, were pretty hard to precisely tailor the pore geometries of scaffolds [32]. On the contrary, the recently developed 3D-printing method could customize the pore parameters as designed, which would be preferable in clinic [32]. Here, BG scaffolds were constructed through an extrusion type 3D-printing. Subsequently, the ultrathin

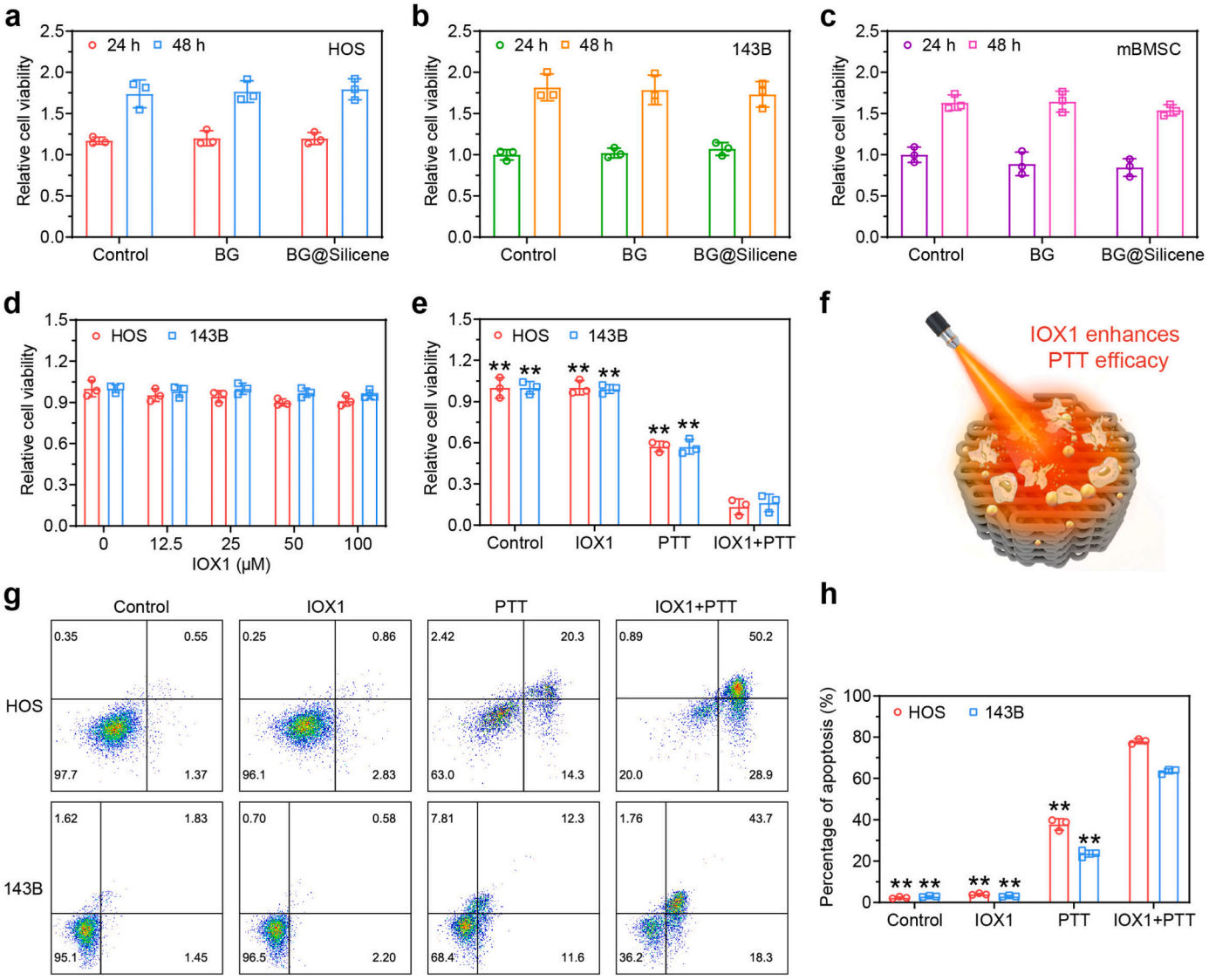

Fig. 4. OS suppression of BG@silicene scaffolds by PTT *in vitro*. Relative viabilities of (a) HOS, (b) 143B cells, and (c) mBMSCs after the indicated treatments for 24 h or 48 h. n = 3. (d) Relative viabilities of OS cells cultured with varying concentrations of IOX1 for 24 h. n = 3. (e) Relative viabilities of OS cells with the indicated treatments. n = 3. (f) Schematic description of IOX1 enhances PTT efficacy of BG@silicene scaffolds. (g, h) The proportion of apoptotic OS cells under the indicated treatments as tested by flow cytometry. n = 3. **p < 0.01 relative to the IOX1 + PTT group.

silicene NSs were fabricated on the BG scaffolds to obtain the BG@silicene scaffolds (Fig. 2c). The loading of silicene NSs endowed the scaffolds with dark color, as visualized in the digital pictures (Fig. 2d). Moreover, the scaffolds featured well-defined macroporous structures as revealed by scanning electron microscopy (SEM) (Fig. 2d). Furthermore, the elemental mapping results presented that P, Si, and Ca elements were in/on the BG@silicene scaffolds as expected (Fig. 2e).

Collectively, the 3D-printing BG@silicene scaffolds were successfully fabricated and ready for further functional evaluations.

3.2. OS suppression of BG@silicene scaffolds by PTT in vitro

Considering that silicene possessed feasible photothermal conversion properties [17,33], the photothermal performance of silicene decorated BG@silicene scaffolds in NIR-II biowindow was further evaluated. As expected, BG@silicene scaffolds elicited a significant temperature promotion when exposed to 1064 nm laser irradiation (Fig. 3a and b). With the exposure time extending, the temperature of BG@silicene significantly elevated in 3 min and kept stable in the next 2 min. Besides the loading amount of silicene NSs, the ultimate stable temperature also depended on the laser power density (Supplementary Fig. S2). Additionally, the photothermal peculiarity of BG@silicene scaffolds kept steady after undergoing five laser-on/off cycles, which was the premise to be developed into a feasible clinic modality (Fig. 3c).

The profound photothermal performance of BG@silicene scaffolds further prompted us to explore their potential cytocompatibility and photothermal therapeutic effects. It is indicated that BG and BG@silicene scaffolds both possessed good biosafety to osteosarcoma cells (HOS and 143B) and mBMSCs, as analyzed by CCK8 assay (Fig. 4a–c). Although much more attention has been drawn to PTT, few have focused on strengthening its therapeutic efficacy while simultaneously avoiding elevating the laser power density since the higher temperature induced by elevating the laser power density would lead to more damage to the surrounding normal tissue. Fortunately, it has been found that the downregulation of lysine demethylase KDM3A would sensitize breast cancer to photothermia epigenetically [17]. Here, IOX1, an inhibitor of histone demethylase KDM3A [23], was introduced to strengthen the therapeutic efficacy of PTT against OS. As shown in Fig. 4d, it turned out that IOX1 alone nearly did not harm OS cells, even to 100 μM. However, the pretreatment of OS cells with IOX1 (50 μM) 24 h before the

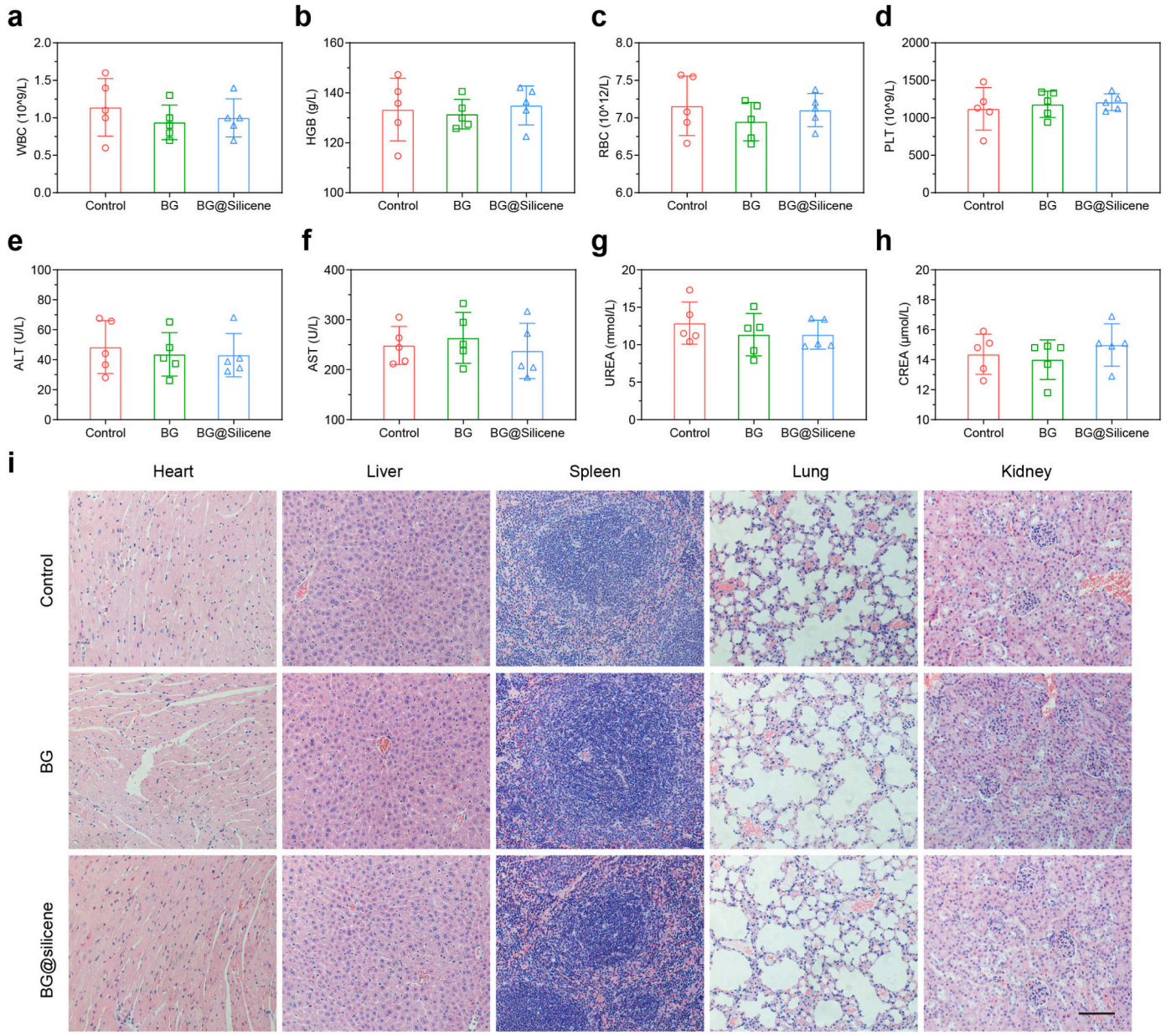

Fig. 5. Biosafety evaluation of BG@silicene scaffolds *in vivo*. (a–h) Hematological and biochemical indexes of the mice with the indicated treatments after 30 days. n = 5. (i) H&E staining images of heart, liver, spleen, lung, and kidney obtained after mice were sacrificed. Scale bar, 100 μm.

execution of laser irradiation (1064 nm, 0.8W·cm^{-2}, 5 min) would sharply enhance the thermal ablation effects (Fig. 4e). More specifically, the relative viabilities of OS cells in control, IOX1 (50 μM), PTT, and IOX1 + PTT groups were about 100%, 100%, 57%, and 15%, respectively, as tested by the CCK8 assay. Similarly, the apoptotic percentage of OS cells in control, IOX1 (50 μM), PTT, and IOX1 + PTT groups were approximately 3%, 4%, 31%, and 71%, respectively, as verified by flow cytometry (Fig. 4f–h).

Taken together, the results indicated that IOX1 could enhance the PTT effects on OS elicited by the biocompatible BG@silicene scaffolds.

3.3. OS elimination induced by IOX1 strengthened PTT of BG@silicene scaffolds in vivo

Inspired by the PTT performance of BG@silicene scaffolds *in vitro*, the therapeutic potential was further investigated *in vivo*. At first, the biosafety of BG or BG@silicene scaffolds was comprehensively evaluated *in vivo*. After being implanted with the BG or BG@silicene scaffolds subcutaneously, the ICR mice were raised under SPF conditions for 30 days. Later, the mice were sacrificed. Their blood and major organs were obtained for thorough analysis. It turned out that there was no significant statistical difference in hematology and blood biochemistry indexes between the untreated control and BG/BG@silicene scaffolds groups, inferring BG/BG@silicene scaffolds did no detective harm to hepatic and renal functions *in vivo* (Fig. 5a–h). Furthermore, the hematoxylin and eosin (H&E) staining results also verified that BG/BG@silicene scaffolds did not cause visible damage to the major organs *in vivo* (Fig. 5i). Combining the hematology and blood biochemistry analyses, the outcomes altogether indicated that BG/BG@silicene scaffolds possessed favorable biocompatibility *in vivo*.

Subsequently, the prompted photothermal performance of BG@silicene scaffolds facilitated by IOX1 was tested in the nude mice xenografts model. In detail, the nude mice were divided randomly into four groups (n = 5): BG + NIR, IOX1 + BG, PTT, and IOX1 + PTT. IOX1 (5 mg·kg^{-1}) was administrated intraperitoneally 20 h before the scaffold implantation surgeries. PTT treatments referred to the combination of

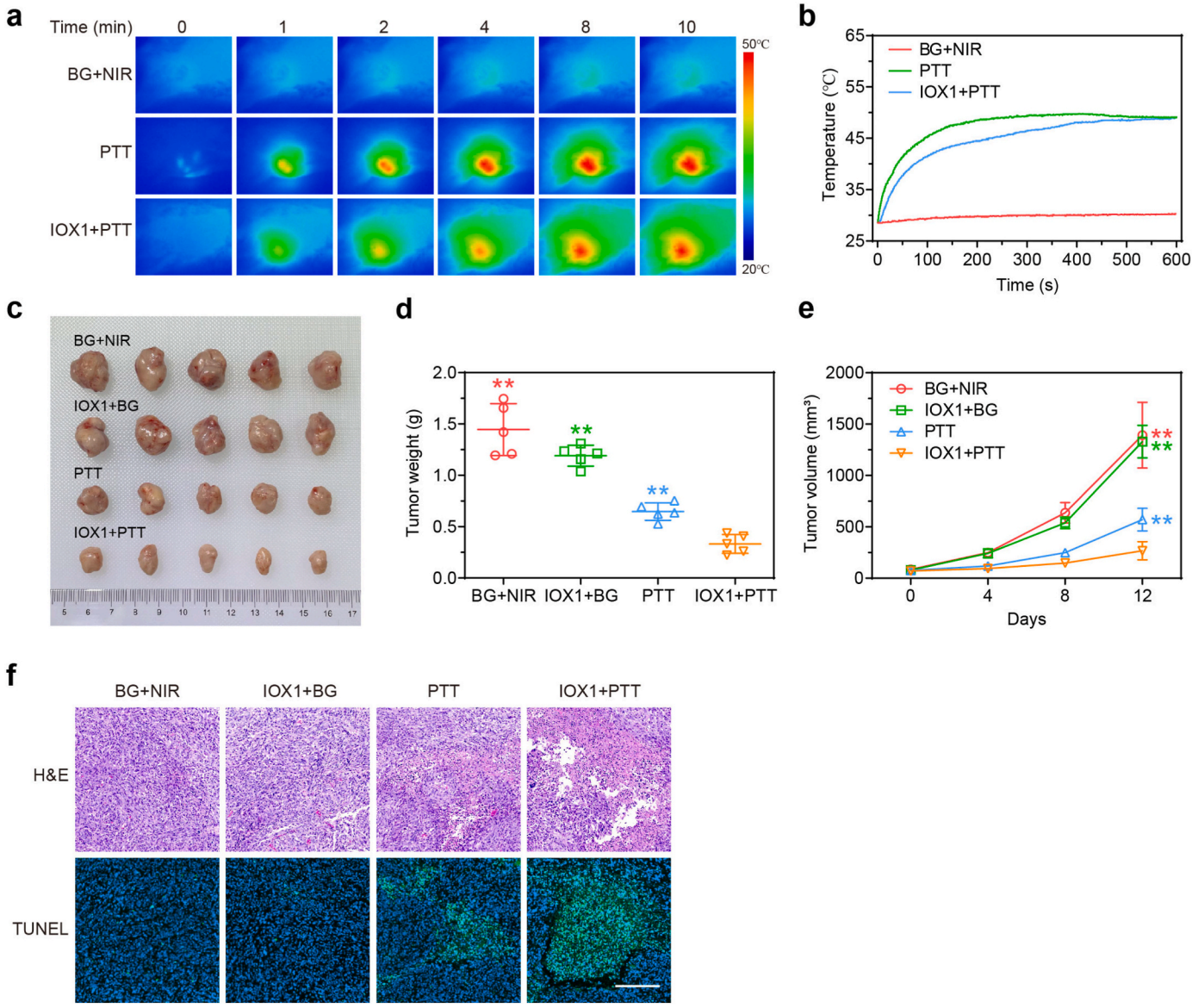

Fig. 6. OS elimination induced by IOX1 strengthened PTT of BG@silicene scaffolds *in vivo*. (a) Infrared thermal photographs of tumor sites and (b) tumor temperature change curves of mice with varied treatments. (c) Digital photos, (d) weights, and (e) volumes of tumors in different groups. n = 5. (f) H&E and TUNEL staining images of typical tumors from each group. Scale bar, 250 μm. **p < 0.01 relative to the IOX1 + PTT group.

BG@silicene scaffold implantation and NIR-II laser irradiation (1064 nm, 0.8 W·cm^{-2}, 10 min); thereinto, laser irradiation was applied 4 h after the implantation of the scaffolds. As expected, under laser irradiation, the temperature at the tumor site was elevated significantly within 6 min in the PTT and IOX1+PTT groups, while the temperature remained nearly unchanged in the BG + NIR group (Fig. 6a and b). Then, tumor volumes were measured every 4 days for 12 days. After the mice were sacrificed, the tumors were resected, photographed, and weighed before being subjected to histochemistry analysis. Compared with the aggressive tumor growth in the BG + NIR and IOX1 + BG groups, the tumors were inhibited significantly in the PTT and IOX1 + PTT groups, mostly in the latter one (Fig. 6c–e and Supplementary Fig. S3). Moreover, the results of H&E indicated that cell fragments were significant in the PTT and IOX1 + PTT groups, mostly in the IOX1 + PTT group (Fig. 6f). In accordance with the H&E results, the outcomes of terminal deoxynucleotidyl transferase dUTP nick-end labeling (TUNEL) staining also lead to the same conclusion, which verified that PTT could efficiently suppress the progression of OS and IOX1 could enhance the inhibitory efficacy of PTT. During the experimental process, neither statistical body weight differences nor behavior abnormalities among the groups were observed, inferring the profound biosafety of the applied therapeutic modalities (Supplementary Fig. S4).

Collectively, the results indicated that the 3D-printing BG@silicene scaffolds presented advanced PTT performance against OS sensitized by IOX1 with favorable biosafety.

3.4. Osteogenesis facilitated by BG@silicene scaffolds in vitro and in vivo

Besides the outstanding photothermal ablation effects, the role that BG@silicene scaffolds played in bone regeneration was then thoroughly tested. It is acknowledged that ALP activity is a typical marker of osteoblast activity in the early stage of osteogenesis [12,20,34]. It turned out that compared with BG scaffolds, BG@silicene scaffolds contributed more to osteogenesis, evidenced by the prompted ALP activity (Fig. 7a). Furthermore, the expression of osteogenesis-related genes (*ALP*, *IBSP*, and *BMP2*) was also upregulated in the BG@silicene scaffolds group on day 7 (Fig. 7b–d). This might benefit from the sustained release of bioactive elements (*e.g.,* calcium, silicon, phosphate, *etc.*), as proved by

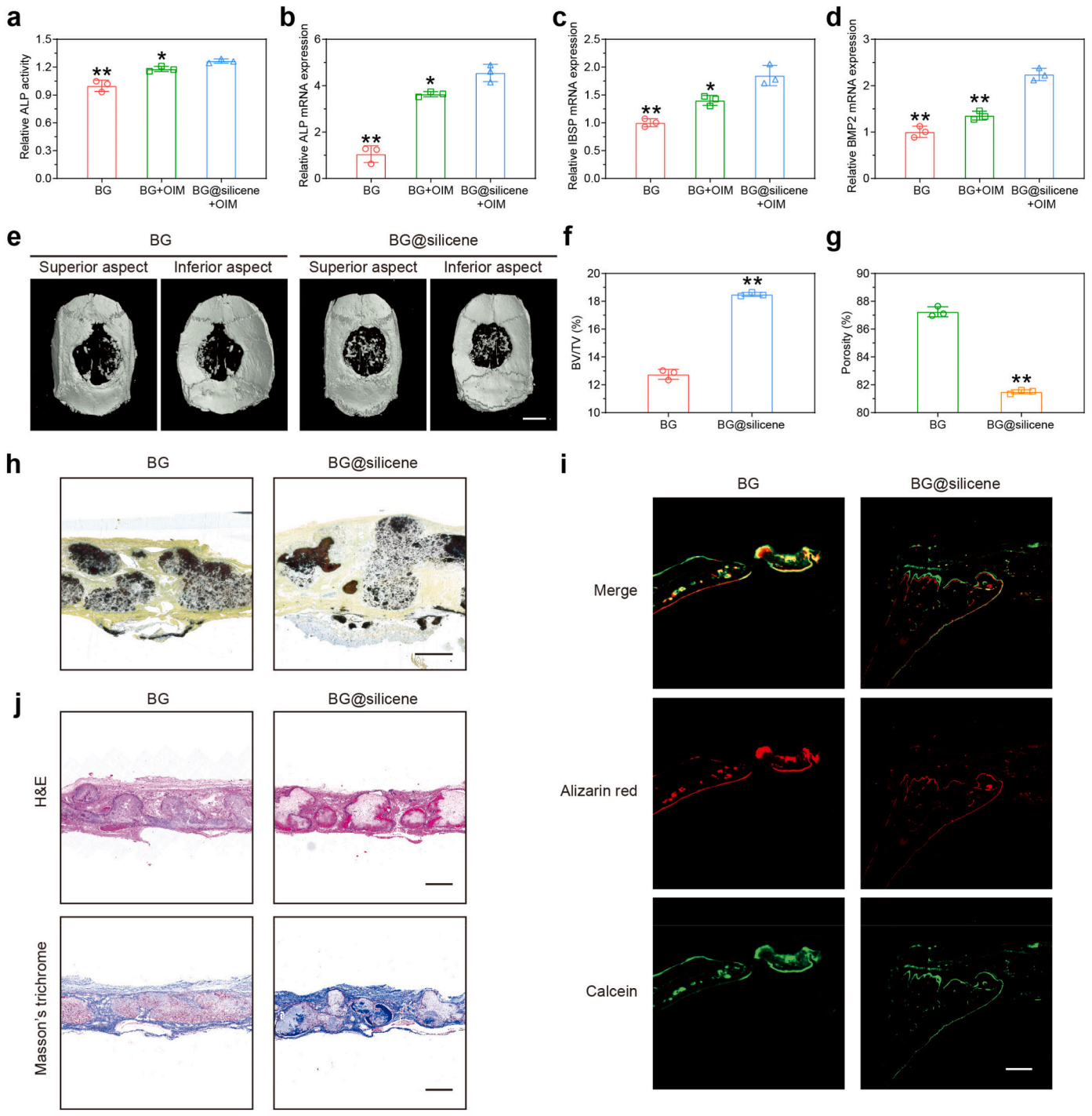

Fig. 7. Osteogenesis facilitated by BG@silicene scaffolds *in vitro* and *in vivo*. (a) Relative ALP activities and (b–d) osteogenic gene expressions (*ALP*, *IBSP*, and *BMP2*) of mBMSCs after different treatments. n = 3. *p < 0.05, **p < 0.01 relative to the BG@silicene + OIM group. (e) 3D reconstruction of the skull based on micro-CT. Scale bar, 4 mm. (f) Bone volume/total volume (BV/TV) and (g) the proportion of porosity in BG and BG@silicene groups. n = 3. **p < 0.01 relative to the BG group. (h) Van Gieson's picrofuchsin staining, (i) confocal fluorescence pictures, as well as (j) H&E and Masson's trichrome staining of the skull deficiency areas in each group. Scale bar, 500 μm.

plenty of previous studies [20].

To further test the osteogenic performance of 3D-printing BG@silicene scaffolds *in vivo*, a rat calvarial defect model was utilized. After 8 weeks, the rats were euthanized, and their skulls were gathered for further analysis. The micro-CT (CT: computed tomography) 3D reconstruction pictures showed the formation of new bone tissues in BG and BG@silicene scaffolds groups, with more in the BG@silicene group, implying the preferable osteogenic property of BG@silicene scaffolds (Fig. 7e). Similarly, higher bone volume/total volume (BV/TV) and lower porosity percentage were achieved in the BG@silicene group compared with the BG group (Fig. 7f and g). In addition, Van Gieson's picrofuchsin staining and the confocal fluorescence images also verified that BG@silicene scaffolds played a more important role in bone regeneration (Fig. 7h and i). Constantly, the histopathological analyses by H&E and Masson's trichrome staining further demonstrated that BG@silicene scaffolds presented superior osteogenic biofunction

compared with BG scaffolds (Fig. 7j). Mechanically, the promoted mineralization of new bone tissue is attributed to the release of bioactive silicon, calcium, and phosphate with the degradation of the BG@silicene scaffolds.

Therefore, the prepared BG@silicene scaffolds, possessing satisfactory biocompatibility, osteoconduction, and osteoinduction, could be developed as a promising bone graft in the future for OS patients.

4. Conclusions

Currently, the treatment of OS encounters great challenges of recurrence [35] and critical bone defects post-surgery [36]. Meanwhile, the survival rates of OS patients have not improved since the 1990s and were far from satisfactory [2,6]. Exploring more efficient and advanced therapeutic strategies against OS is pivotal to promoting prognosis and benefiting the patients. Hereinto, developing distinct biocompatible platforms with dual-functions of OS elimination and osteogenesis would be preferable and promising for future clinical translation [37,38].

In this work, we successfully constructed a biocompatible, biodegradable silicene NSs-loaded 3D-printing BG scaffold (BG@silicene) as a potential therapeutic implant, which suppressed OS progression assisted by IOX1 in NIR-II biowindow and achieved profound osteogenesis *in vitro* and *in vivo*.

Impressively, before the execution of PTT, IOX1 was administrated to sensitize OS to the forthcoming PTT, which gave an example of utilizing epigenetic modulation agents to optimize PTT effects further and minimize associated adverse/side effects. IOX1 is a known broad-spectrum inhibitor of 2-oxoglutarate oxygenase, especially against KDM3A [23]. Studies have demonstrated that IOX1 presented inhibitory effects on HeLa cells, hepatocellular carcinoma, β-thalassemia, and vascular smooth muscle cells, but no one has reported its impacts on OS or PTT [39–42].

On the other hand, although most bone defects can be cured using autologous bone grafting as the gold standard technique, the limited donor sites and the potential complications restrict its wide application and expansion [43]. More personalized, operable, and bioactive alterations needed to be developed to meet the increasing clinical needs. Nowadays, 3D-printing plays a more critical role in bone tissue engineering owing to its customized and adjustable characteristics [44]. Compared with the scaffolds obtained by traditional techniques such as freeze-drying, gas foaming, and electrospinning, 3D-printing can accurately modulate the pore geometries, connectivity, porosity, components, and mechanical properties of scaffolds [45–48], endowing the scaffolds with better bioactive functions on bone regeneration [49]. Meanwhile, gradually releasing bioactive components (*e.g.*, calcium, silicon, phosphate, *etc*.) from the degradation of BG@silicene scaffolds would further stimulate osseous regeneration. Moreover, the 3D-printing scaffolds with a designed shape and interconnected porosity provided possibilities for the fabrication of preferable patient-customized implants.

Taken together, the developed BG@silicene scaffolds were highly promising in future clinical translation to eliminate OS by enhanced PTT assisted by IOX1 and facilitate bone formation as revealed *in vitro* and *in vivo*.

CRediT authorship contribution statement

Yimin Liang: Conceptualization, Data curation, Formal analysis, Methodology. **Chunmeng Wang:** Conceptualization, Data curation, Software. **Shiyang Yu:** Conceptualization, Investigation, Methodology. **Yujia Fan:** Methodology, Software. **Yuhang Jiang:** Supervision. **Renpeng Zhou:** Conceptualization, Formal analysis, Supervision, Visualization, Writing - review & editing. **Wangjun Yan:** Conceptualization, Methodology, Supervision, Visualization, Writing - review & editing. **Yangbai Sun:** Conceptualization, Data curation, Funding acquisition, Investigation, Visualization, Writing - original draft, Writing - review & editing.

Declaration of competing interest

The authors declare that they have no known competing financial interests or personal relationships that could have appeared to influence the work reported in this paper.

Data availability

Data will be made available on request.

Acknowledgements

All animal experimental protocols were performed following the relevant guidelines and approved by the Ethics Committee of Shanghai Medical College Fudan University. The research was supported by Shanghai Municipal Health Commission Research Project (Grant No. 20194Y0242) and National Natural Science Foundation of China (Grant No. 82372525).

Appendix A. Supplementary data

Supplementary data to this article can be found online at https://doi.org/10.1016/j.mtbio.2023.100887.

References

[1] D.M. Gianferante, L. Mirabello, S.A. Savage, Germline and somatic genetics of osteosarcoma-connecting aetiology, biology and therapy, Nat. Rev. Endocrinol. 13 (2017) 480–491.
[2] E. Simpson, H.L. Brown, Understanding osteosarcomas, J. Am. Acad. Physician Assistants 31 (2018) 15–19.
[3] J.L. Ferguson, S.P. Turner, Bone cancer: diagnosis and treatment principles, Am. Fam. Physician 98 (2018) 205–213.
[4] A. Luetke, P.A. Meyers, I. Lewis, H. Juergens, Osteosarcoma treatment - where do we stand? A state of the art review, Cancer Treat Rev. 40 (2014) 523–532.
[5] Y. Wang, J. Wang, H. Hao, M. Cai, S. Wang, J. Ma, Y. Li, C. Mao, S. Zhang, In vitro and in vivo mechanism of bone tumor inhibition by selenium-doped bone mineral nanoparticles, ACS Nano 10 (2016) 9927–9937.
[6] K. Berner, T.B. Johannesen, A. Berner, H.K. Haugland, B. Bjerkehagen, P.J. Bohler, O.S. Bruland, Time-trends on incidence and survival in a nationwide and unselected cohort of patients with skeletal osteosarcoma, Acta Oncol. (Madr.) 54 (2015) 25–33.
[7] M. Heng, A. Gupta, P.W. Chung, J.H. Healey, M. Vaynrub, P.S. Rose, M.T. Houdek, P.P. Lin, A.J. Bishop, F.J. Hornicek, Y.L. Chen, S. Lozano-Calderon, G.E. Holt, I. Han, D. Biau, X. Niu, N.M. Bernthal, P.C. Ferguson, J.S. Wunder, T. Ueda, S. Kakunaga, A. Kawai, H. Sugiura, T. Kidani, T. Kunisasa, T. Ozaki, K. Ae, A. Nagano, T. Ohno, K. Hiraoka, N. Yamamoto, H. Tsuchiya, Y. Matsumoto, T. Yanagawa, R. Nakayama, H. Morioka, T. Kubo, S. Simose, Y. Yamagami, T. Yamamoto, M. Kawasaki, T. Torigoe, Y. Yazawa, T. Akiyama, T. Gokita, J. Manabe, M. Kaya, M. Emori, T. Nakamura, A. Matsumine, S. Sugihara, M. Yokouchi, S. Komiya, Y. Suehara, T. Takagi, T. Kawamoto, J. Wasa, T. Yonemoto, T. Ishii, I. Baba, M. Hoshi, K. Hamada, N. Naka, T. Sotobori, N. Araki, T. Okuma, T. Goto, H. Kobayashi, H. Kawano, M. Hosaka, H. Futani, H. Hiraga, Y. Nishida, A. Griffin, A.R.A. Razak, D.B. Shultz, C. Catton, S. Robinson, S.R. Patel, V.O. Lewis, B.A. Guadagnolo, T. DeLaney, H. Wang, K. Raskin, A.K. Callan, R. Henshaw, M. Isler, S. Mottard, W.M. Chen, F. Traub, T.W.W. Chen, R. E. Turcotte, D. Davidson, P.U. Tunn, H. Loong, M. Ghert, J. Werier, P. Clarkson, J. A. Abraham, The role of chemotherapy and radiotherapy in localized extraskeletal osteosarcoma, Eur. J. Cancer 125 (2020) 130–141.
[8] K. Zhang, Y. Zhou, C. Xiao, W. Zhao, H. Wu, J. Tang, Z. Li, S. Yu, X. Li, L. Min, C. Tu, X. Zhang, Application of hydroxyapatite nanoparticles in tumor-associated bone segmental defect, Sci. Adv. 5 (2019), eaax6946.
[9] L. Ma, X. Feng, H. Liang, K. Wang, Y. Song, L. Tan, B. Wang, R. Luo, Z. Liao, G. Li, S. Wu, C. Yang, A novel photothermally controlled multifunctional scaffold for clinical treatment of osteosarcoma and tissue regeneration, Mater. Today 36 (2020) 48–62.
[10] Y. Liu, P. Bhattarai, Z. Dai, X. Chen, Photothermal therapy and photoacoustic imaging: via nanotheranostics in fighting cancer, Chem. Soc. Rev. 48 (2019) 2053–2108.
[11] C. He, L. Yu, L. Ding, Y. Chen, Y. Hao, Self-assembled/drug-composed nanomedicine for synergistic photonic hyperthermia and targeted therapy of breast cancer by inhibiting ERK, AKT, and STAT3 signaling cascades, Adv. Funct. Mater. 30 (2020), 1908907.
[12] C. He, C. Dong, L. Yu, Y. Chen, Y. Hao, Ultrathin 2D inorganic ancient pigment decorated 3D-printing scaffold enables photonic hyperthermia of osteosarcoma in

NIR-II biowindow and concurrently augments bone regeneration, Adv. Sci. 8 (2021), 2101739.
[13] A.C.V. Doughty, A.R. Hoover, E. Layton, C.K. Murray, E.W. Howard, W.R. Chen, Nanomaterial applications in photothermal therapy for cancer, Materials 12 (2019) 779.
[14] P. Ares, K.S. Novoselov, Recent advances in graphene and other 2D materials, Nano Mater. Sci. 4 (2022) 3–9.
[15] N. Mamidi, M.R. Martínez Gamero, R.M. Velasco Delgadillo, J.V. Castrejón, A. E. Zúníga, Engineering of functionalized carbon nano-onions reinforced nanocomposites: fabrication, biocompatibility, and mechanical properties, J. Mater. Res. 35 (2020) 922–930.
[16] S.J. Soenen, P. Rivera-Gil, J.-M. Montenegro, W.J. Parak, S.C. De Smedt, K. Braeckmans, Cellular toxicity of inorganic nanoparticles: common aspects and guidelines for improved nanotoxicity evaluation, Nano Today 6 (2011) 446–465.
[17] C. He, L. Yu, L. Ding, H. Yao, Y. Chen, Y. Hao, Lysine demethylase KDM3A regulates nanophotonic hyperthermia resistance generated by 2D silicene in breast cancer, Biomaterials 255 (2020), 120181.
[18] Y. Zhang, T. Song, T. Feng, Y. Wan, N.T. Blum, C. Liu, C. Zheng, Z. Zhao, T. Jiang, J. Wang, L. Tang, P. Huang, Plasmonic modulation of gold nanotheranostics for targeted NIR-II photothermal-augmented immunotherapy, Nano Today 35 (2020), 100987.
[19] Q. Xin, H. Ma, H. Wang, X.-D. Zhang, Tracking tumor heterogeneity and progression with near-infrared II fluorophores, Explorations 3 (2023), 20220011.
[20] C. He, L. Yu, H. Yao, Y. Chen, Y. Hao, Combinatorial photothermal 3D-printing scaffold and checkpoint blockade inhibits growth/Metastasis of breast cancer to bone and accelerates osteogenesis, Adv. Funct. Mater. 31 (2020), 2006214.
[21] L.-H. Fu, C. Qi, T. Sun, K. Huang, J. Lin, P. Huang, Glucose oxidase-instructed biomineralization of calcium-based biomaterials for biomedical applications, Explorations 00 (2023), 20210110.
[22] Y. Liang, H. Wu, Z. Lin, Q. Liu, Z. Zhang, 3D printed aluminum matrix composites with well-defined ordered structures of shear-induced aligned carbon fibers, Nano Mater. Sci. 4 (2022) 366–375.
[23] J. Liu, Z. Zhao, N. Qiu, Q. Zhou, G. Wang, H. Jiang, Y. Piao, Z. Zhou, J. Tang, Y. Shen, Co-delivery of IOX1 and doxorubicin for antibody-independent cancer chemo-immunotherapy, Nat. Commun. 12 (2021) 2425.
[24] P. Srinath, P. Abdul Azeem, K. Venugopal Reddy, Review on calcium silicate-based bioceramics in bone tissue engineering, Int. J. Appl. Ceram. Technol. 17 (2020) 2450–2464.
[25] L. Zhou, J. Lyu, F. Liu, Y. Su, L. Feng, X. Zhang, Immunogenic PANoptosis-initiated cancer sono-immune reediting nanotherapy by iteratively boosting cancer immunity cycle, Adv. Mater. 12 (2023), 2305361.
[26] L. Zhou, W. Feng, L. Chen, H. Huang, S. Huang, Q. Chen, X. Zhang, Y. Chen, Targeting acidogenic metabolism by engineering self-catalytic siRNA nanocarriers/nanocatalysts for amplified tumor apoptosis/ferroptosis, Nano Today 46 (2022), 101623.
[27] L. Zhou, W. Feng, Y. Mao, Y. Chen, X. Zhang, Nanoengineered sonosensitive platelets for synergistically augmented sonodynamic tumor therapy by glutamine deprivation and cascading thrombosis, Bioact. Mater. 24 (2023) 26–36.
[28] C. He, C. Liu, L. Wang, Y. Sun, Y. Jiang, Y. Hao, Histone methyltransferase NSD2 regulates apoptosis and chemosensitivity in osteosarcoma, Cell Death Dis. 10 (2019) 65.
[29] C. He, J. Sun, C. Liu, Y. Jiang, Y. Hao, Elevated H3K27me3 levels sensitize osteosarcoma to cisplatin, Clin. Epigenet. 11 (2019) 8.
[30] C. He, Z. Sun, R.M. Hoffman, Z. Yang, Y. Jiang, L. Wang, Y. Hao, P-glycoprotein overexpression is associated with cisplatin resistance in human osteosarcoma, Anticancer Res. 39 (2019) 1711–1718.
[31] C. Feng, W. Zhang, C. Deng, G. Li, J. Chang, Z. Zhang, X. Jiang, C. Wu, 3D printing of Lotus root-like biomimetic materials for cell delivery and tissue regeneration, Adv. Sci. 4 (2017), 1700401.
[32] H. Autefage, F. Allen, H.M. Tang, C. Kallepitis, E. Gentleman, N. Reznikov, K. Nitiputri, A. Nommeots-Nomm, M.D. O'Donnell, C. Lange, G. Blunn, M. M. Stevens, Multiscale analyses reveal native-like lamellar bone repair and near perfect bone-contact with porous strontium-loaded bioactive glass, Biomaterials 209 (2019) 152–162.
[33] H. Lin, W. Qiu, J. Liu, L. Yu, S. Gao, H. Yao, Y. Chen, J. Shi, Silicene: wet-chemical exfoliation synthesis and biodegradable tumor nanomedicine, Adv. Mater. 31 (2019), 1903013.
[34] C. He, C. Dong, H. Hu, L. Yu, Y. Chen, Y. Hao, Photosynthetic oxygen-self-generated 3D-printing microbial scaffold enhances osteosarcoma elimination and prompts bone regeneration, Nano Today 41 (2021), 101297.
[35] C. He, Y. Jiang, Y. Guo, Z. Wu, Amplified ferroptosis and apoptosis facilitated by differentiation therapy efficiently suppress the progression of osteosarcoma, Small 19 (2023), 2302575.
[36] J. Zhou, Z. Zhang, J. Joseph, X. Zhang, B.E. Ferdows, D.N. Patel, W. Chen, G. Banfi, R. Molinaro, D. Cosco, N. Kong, N. Joshi, O.C. Farokhzad, C. Corbo, W. Tao, Biomaterials and nanomedicine for bone regeneration: progress and future prospects, Explorations 1 (2021), 20210011.
[37] L. Ma, J. Zhou, Q. Wu, G. Luo, M. Zhao, G. Zhong, Y. Zheng, X. Meng, S. Cheng, Y. Zhang, Multifunctional 3D-printed scaffolds eradiate orthotopic osteosarcoma and promote osteogenesis via microwave thermo-chemotherapy combined with immunotherapy, Biomaterials 301 (2023), 122236.
[38] C. Xu, Y. Xia, P. Zhuang, W. Liu, C. Mu, Z. Liu, J. Wang, L. Chen, H. Dai, Z. Luo, FePSe3-Nanosheets-Integrated cryogenic-3D-printed multifunctional calcium phosphate scaffolds for synergistic therapy of osteosarcoma, Small 19 (2023), 2303636.
[39] H.J. Ahn, S.Y. Hwang, N.H. Nguyen, I.J. Lee, E.J. Lee, J. Seong, J.S. Lee, Radiation-induced CXCL12 upregulation via histone modification at the promoter in the tumor microenvironment of hepatocellular carcinoma, Mol. Cell. 42 (2019) 530–545.
[40] R.J. Hopkinson, A. Tumber, C. Yapp, R. Chowdhury, W.S. Aik, K.H. Che, X.S. Li, J. B.L. Kristensen, O.N.F. King, M.C. Chan, K.K. Yeoh, H. Choi, L.J. Walport, C. C. Thinnes, J.T. Bush, C. Lejeune, A.M. Rydzik, N.R. Rose, E.A. Bagg, M. A. McDonough, T.J. Krojer, W.W. Yue, S.S. Ng, L. Olsen, P.E. Brennan, U. Oppermann, S. Müller, R.J. Klose, P.J. Ratcliffe, C.J. Schofield, A. Kawamura, 5-Carboxy-8-hydroxyquinoline is a broad spectrum 2-oxoglutarate oxygenase inhibitor which causes iron translocation, Chem. Sci. 4 (2013) 3110–3117.
[41] S. Mettananda, C.A. Fisher, J.A. Sloane-Stanley, S. Taylor, U. Oppermann, R. J. Gibbons, D.R. Higgs, Selective silencing of α-globin by the histone demethylase inhibitor IOX1: a potentially new pathway for treatment of β-thalassemia, Haematologica 102 (2017) e80–e84.
[42] Q. Hu, J. Chen, J. Zhang, C. Xu, S. Yang, H. Jiang, IOX1, a JMJD2A inhibitor, suppresses the proliferation and migration of vascular smooth muscle cells induced by angiotensin II by regulating the expression of cell cycle-related proteins, Int. J. Mol. Med. 37 (2016) 189–196.
[43] X. Wang, D. Zhang, F. Zhang, L. Jin, D. Shi, Z. Hou, Effect analysis of iliac bone autografting for Hepple V osteochondral lesions of the talus, J. Orthop. Surg. Res. 17 (2022) 33.
[44] W. Dang, B. Ma, B. Li, Z. Huan, N. Ma, H. Zhu, J. Chang, Y. Xiao, C. Wu, 3D printing of metal-organic framework nanosheets-structured scaffolds with tumor therapy and bone construction, Biofabrication 12 (2020), 025005.
[45] L. Zhang, G. Yang, B.N. Johnson, X. Jia, Three-dimensional (3D) printed scaffold and material selection for bone repair, Acta Biomater. 84 (2019) 16–33.
[46] S.L. Sing, F.E. Wiria, W.Y. Yeong, Selective laser melting of titanium alloy with 50 wt% tantalum: effect of laser process parameters on part quality, Int. J. Refract. Met. Hard Mater. 77 (2018) 120–127.
[47] H. Wang, K. Su, L. Su, P. Liang, P. Ji, C. Wang, Comparison of 3D-printed porous tantalum and titanium scaffolds on osteointegration and osteogenesis, Mater. Sci. Eng. C 104 (2019), 109908.
[48] S. Bose, S. Vahabzadeh, A. Bandyopadhyay, Bone tissue engineering using 3D printing, Mater. Today 16 (2013) 496–504.
[49] V. Karageorgiou, D. Kaplan, Porosity of 3D biomaterial scaffolds and osteogenesis, Biomaterials 26 (2005) 5474–5491.